Biosensors and Bioelectronics 129 (2019) 100–106

Contents lists available at ScienceDirect

Biosensors and Bioelectronics

journal homepage: www.elsevier.com/locate/bios

Electrochemiluminecence nanogears aptasensor based on MIL-53(Fe)@CdS for multiplexed detection of kanamycin and neomycin

Defen Feng[a], Xuecai Tan[a,*], Yeyu Wu[a,*], Chenhao Ai[a], Yanni Luo[a], Quanyou Chen[a], Heyou Han[b]

[a] School of Chemistry and Chemical Engineering, Guangxi University for Nationalities, Guangxi Key Laboratory of Chemistry and Engineering of Forest Products, Key Laboratory of Guangxi Colleges and Universities for Food Safety and Pharmaceutical Analytical Chemistry, Nanning 530008, China

[b] State Key Laboratory of Agricultural Microbiology, College of Science, College of Food Science and Technology, Huazhong Agricultural University, Wuhan 430070, China

ARTICLE INFO

Keywords:
Electrochemiluminescence
Electrochemiluminecence resonance energy transfer
Surface plasmon resonance
Nanogears
Antibiotic

ABSTRACT

A dual gears electrochemiluminecence (ECL) aptasensing strategy for multiple selective determination of kanamycin and neocycin was designed on the basis of the combination of kanamycin and neocycin induced dual gears conversion, the loading platform of metal-organic frameworks (MOFs), surface plasmon resonance (SPR) and ECL resonance energy transfer (ERET) between CdS QDs and AuNPs (or PtNPs). In the absence of target, the dual gears were "off". Then the B1-AuNP (gear B) and aptamer 1-PtNPs acted as signal quenching elements to quench ECL intensity due to ERET process. Upon addition of kanamycin, the aptamer 1-PtNPs were removed from the gear gradually, the ECL was enhanced due to SPR process between AuNPs and CdS QDs. After the incubation of aptamer 2, the dual gears were "off" again and ECL intensity was decreased by ERET process between AuNPs and CdS QDs. In the presence of neomycin, dual gears were "on" again, the ECL signal was enhanced by SPR process between AuNPs and CdS QDs. Under optimal condition, the proposed aptasensor exhibited wide linear ranges of kanamycin (10^{-10}–10^{-6} M) and neomycin (10^{-9}–10^{-5} M), and relatively low detection limits to kanamycin (1.7×10^{-11} M) and neomycin (3.5×10^{-10} M). The developed aptasensor realized the multiple ECL detection of kanamycin and neomycin with single luminophore, and was successfully applied to the detection of kanamycin and neomycin in food samples.

1. Introduction

In the field of food safety studies, it is significance to develop selective, sensitive and simple assays for multiple antibiotic residues detection from complex food matrices. Kanamycin and neomycin were aminoglycoside antibiotics, that were active against Gram-negative and Gram-positive bacteria, including Pseudomonas and Proteus et al. (Oertel et al., 2004). However, aminoglycoside antibiotic presents well-known potentially cochlear, vestibular toxicity and nephrotoxicity to human and animals, which results in failure to return to work and reduced quality of life (Lian et al., 2013). During the past decades, many methods have been developed for the determination of kanamycin and neomycin including photoelectrochemical (Lv et al., 2017), high performance liquid chromatography-mass spectrometry (LC-MS) (Perez and Chen, 2018; Zu et al., 2018), colorimetric (Zhou et al., 2013; Ha et al., 2017) and luminescent (Leung et al., 2013). But those methods present disadvantages of time consuming operation, tedious pre-processing process (LC-MS), low sensitivity (colorimetric), narrow linear range (photoelectrochemical), and because the structures and properties of kanamycin and neomycin are similar, these sensor methods couldn't directly distinguish them. Therefore, it is necessary for us to develop a quick and sensitive method for the detection of multiple antibiotic residues in foodstuffs from animals.

Electrochemiluminecence (ECL) is a light emission process in which electrochemically triggered optical radiation process produced by the energy relaxation of excited species (Li et al., 2017). This method has attracted considerable attention due to its high sensitivity, low background response and rapid response (Richter, 2004). As we all know, only one target was detected by traditional ECL instrument due to the limited of a single optical signal. Nowadays, researchers used two luminophores or multivariate linear algebraic equations based on introducing different ECL probes to achieve multiple detections, these methods either cannot eliminate the cross-reaction of different ECL probes or required to abundant laboratory data and establish composite mathematical model (Han et al., 2014; Liang et al., 2016). In consequence, it is an urgent challenge to develop a feasible strategy, which realizing multivariate antibiotics detection with single ECL luminophore and regenerating the sensing platform. ECL aptasensor is one of

* Correspondence to: Guangxi University for Nationalities, Nanning 530008, China.
E-mail addresses: gxunxctan@126.com (X. Tan), eveyeyu@163.com (Y. Wu).

https://doi.org/10.1016/j.bios.2018.12.050
Received 27 October 2018; Received in revised form 19 December 2018; Accepted 28 December 2018
Available online 09 January 2019
0956-5663/

the ways to achieve multivariate antibiotics detection with single ECL luminophore. Aptamer is short single-stranded oligonucleotide, which bind to target analytes via the formation of a specific tertiary structure. Aptamer has been increasingly advocated as alternatives to antibodies due to its low cost, high stability and inherent selectivity (Zhao et al., 2014). In recent years, DNA nanorobotics such as “spiders”, “gears” and “tweezers” have been captured considerable attractions due to the advantage of predictable conformation and programmable intra and intermolecular Watson-Crick base-pairing interactions (Wang et al., 2011; Zhang et al., 2014). “Gears” have circular DNA molecule, it can rotate one against another with sufficient external stimulation (Tian and Mao, 2004).

ECL resonance energy transfer (ERET) is inspired by Förster resonance energy transfer (FRET), which depends on the overlap of absorption and emission spectral, as well as the distance (10 ± 2 nm) between the energy donor and acceptor (Fan et al., 2015). Semiconductor quantum dots (QDs), which have proved to be the promising ECL emitters due to broad excitation, tunable emission wavelength and binding compatibility with biomolecules (Miao, 2008; Deng et al., 2014). Nanostructural metallic, especially Au nanoparticles (AuNPs) and Pt nanoparticles (PtNPs), were widely used as ECL energy acceptors due to their strong surface plasmon resonance (SPR), broad absorption spectra and high extinction coefficient (Jin and Gao, 2009). Previous studies have demonstrated that CdS QDs was an ECL luminophore, while nanostructural metallic (AuNPs or PtNPs) can act as ECL quencher or ECL enhancer to the QDs luminophore. When the luminophores and nanostructure metallic are at close proximity, ECL signal was quenched by ERET (Neumann et al., 2002). On the other hand, ECL signal was enhanced due to the SPR between luminophores and nanostructure metallic (Stokes et al., 2007).

In order to fabricate a sensor based on ERET (or SPR) between QDs and nanostructural metallic (AuNPs or PtNPs), it is important to use some suitable material to load QDs for signal development and amplification. Metal-organic frameworks (MOFs) are ideal candidate, which present nice monodispersity and larger specific area are suitable for the assembly of sensor and loading QDs (Eddaoudi et al., 2002; Li et al., 1999). MIL-53(Fe)@CdS QDs could increase the immobilized amount and the stability of QDs due to the large specific area and stable structure of MIL-53(Fe), which improved the sensitivity and stability of ECL aptasensor in a certain extent (Xiong et al., 2017).

Here we demonstrate a dual gears ECL aptasensing platform for specific detection of antibiotic targets with MIL-53(Fe)@CdS-PEI as the ECL luminophores and nanostructural metallic (AuNPs or PtNPs) functioning as both ECL quencher and enhancer. Via the delivery mode of dual gears to realize detection of multiple antibiotics, and the sensor underwent ERET (or SPR) process between CdS QDs and nanostructure metallic (Scheme 1). In this work, MIL-53(Fe) has excellent conductivity and large surface area which acted as the loading platform of CdS QDs. In particular, thioglycolic acid-stabilized CdS QDs introduces a large number of carboxyl groups, which are beneficial to the amidation between CdS QDs and PEI to realize the synthesis of MIL-53(Fe) @CdS-PEI composite. This composite was dropped onto sensor surface as backing material, due to its excellent electrical conductivity and broad excitation. Then nanostructure metallic modified gears and aptamers were modified the electrode by stepwise assembly by the principle of complementary base pairing. In the absence of target, the dual gears were "off", and ECL intensity was low due to an ERET process. Upon addition of kanamycin, the ECL intensity was enhanced because SPR processed between AuNPs and CdS QDs. When aptamer 2 was combined with the modified electrode, dual gears were "off" again, and ECL intensity was decreased via ERET between AuNPs and CdS QDs. Following, neomycin was introduced to fully hybridize with aptamer 2, aptamer 2 was removed from the gear gradually. Dual gears were "on", and thus enhance the ECL intensity by SPR processed between AuNPs and CdS QDs. This aptasensor realized the multiple ECL detection of kanamycin and neomycin with single luminophore, and was successfully applied to the detection of kanamycin and neomycin in food samples with a wide linear range and low detection limit.

2. Experimental section

2.1. Fabrication and detection process of ECL aptasensor

Synthesis of MIL-53(Fe), TGA-capped CdS QDs and MIL-53(Fe) @CdS-PEI was illustrated as S2 and S3 in Supporting information. And, preparation of AuNPs-B1, aptamer 1-PtNPs, gear A and gear B was illustrated as S3 and S4 in Supporting information.

For electrode modification, GCE was polished with 1.0, 0.3 and 0.05 μm alumina powder respectively, then rinsed with water, achieving a mirror-like surface. MIL-53(Fe)@CdS was dropped onto the surface of GCE and dry at room temperature. Then, 150 μL mixture (0.3 mM ECD and 0.1 mM NHS) was added into 50 μL gear A to activate the carboxyl groups for 1 h at room temperature. Electrode was modified with 20 μL gear A mixture through amide bonds at 4 °C for 12 h, and then was rinsed with PBS solution. Next, the modified electrode was blocked with 10 μL 1% BSA at room temperature for 1 h and rinsed with PBS thoroughly. Subsequently, the electrode was successively incubated with aptamer 1-PtNPs, gear B and 20 μL of L1 at room temperature for 1 h, and rinsed with PBS after each incubation step. So the fabrication of dual antibiotic-DNA nanogear was completed (Scheme 1). When not in used, the aptasensor was stored at 4 °C.

When detection, 20 μL different concentrations of kanamycin was dropped onto the surface of aptasensor at room temperature for 1 h and rinsed with PBS, the electrodes were placed in an ECL instrument for signal detection in 0.1 M PBS (pH 7.4) containing 0.01 M $K_2S_2O_8$. Then, electrode was modified with aptamer 2 at room temperature for 1 h and rinsed with PBS. Then electrode was incubated with 20 μL different concentrations of neomycin at room temperature for 1 h and rinsed with PBS, then used an ECL instrument for neomycin detection in 0.1 M PBS (pH 7.4) containing 0.01 M $K_2S_2O_8$.

2.2. Sample preparation

Milk and honey samples were purchased from a local market in China and kept at 4 °C before analysis. The preparation method of milk sample was referred to the literature with some modification (Wu et al., 2014). 1 mL 10^{-7} M of kanamycin (neomycin) standard solution added into lowfat milk, and 30 g of ammonium sulfate was added into the mixture under stirring to precipitate proteins and fats of milk for 30 min. Subsequently, centrifuged at 12,000 rpm for 10 min at 4 °C to collect filtrate. Finally, the supernatant was filtered through a 0.22 μm PTFE membrane, and diluted to 100 mL with water. The blank sample was prepared in the same way but without antibiotic added.

For the honey sample preparation, 1 mL 10^{-7} M of kanamycin (neomycin) standard solution and 10 mL 0.1 M PBS were added to 1 g of honey, then was mixed with a vortex mixer. Subsequently, the solution was centrifuged at 10,000 rpm for 15 min, then the supernatant was filtered through a 0.22 μm PTFE membrane, diluted to a 100 mL with water (Thongchai et al., 2010). The blank sample was prepared in the same way but without antibiotic added.

3. Results and discussion

3.1. Characterization of MIL-53(Fe), CdS QDs, AuNPs, PtNPs and CdS QDs-PEI

MIL-53(Fe) and MIL-53(Fe)@CdS-PEI were characterized by SEM; CdS QDs, AuNPs, PtNPs by were characterized by SEM and TEM (Fig. S1). As shown in Fig. S1A, the MIL-53(Fe) particle was irregular lump with length less than 20 μm. The SEM and TEM images of CdS QDs showed a circular structure with an average diameter of 5 ± 1 nm (Fig. S1B). The SEM and TEM results of AuNPs performed the average

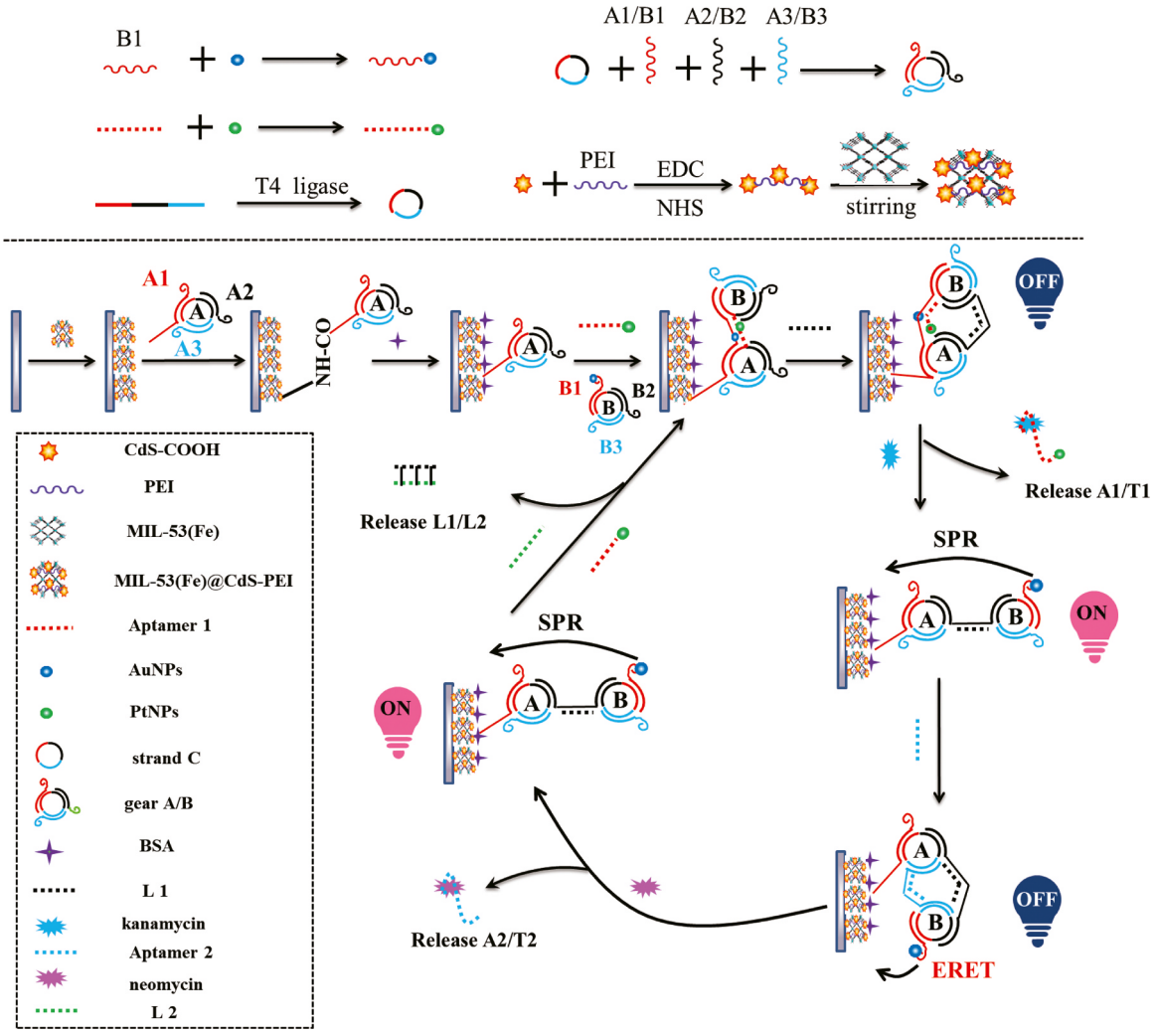

Scheme 1. Schematic representation of an ECL aptasensor for kanamycin and neomycin detection.

diameter was 5 ± 1 nm (Fig. S1C). In Fig. S1D, the prepared PtNPs particles presented diameter less than 10 nm. As Fig. S1E shown, CdS QDs particles were uniform distribution in the CdS-PEI composite. Also, CdS-PEI was evenly distributed on the surface of MIL-53(Fe) (Fig. S1F).

X-ray powder diffraction patterns were characterized to confirm the successfully synthesized of composite. As shown in Fig. 1A, the XRD pattern of the synthesized MIL-53(Fe) was basically corresponded to he simulated one. XRD data of CdS QDs had three strong peaks at 26.6°, 44.0° and 52.2° which corresponded to the (111), (220) and (311) crystal planes of cubic CdS QDs, respectively. For the MIL-53(Fe)@CdS-PEI composite, the XRD characteristic peaks of MIL-53(Fe) was retained, but the peaks of CdS QDs were unapparent mainly due to PEI polymer decreased the diffraction. As shown in Fig. 1B, MIL-53(Fe) @CdS QDs-PEI had more amine that can be used to bond with carboxyl of aptamer. Compared to CdS QDs (Fig. 2B curve a), CdS QDs-PEI (Fig. 2B curve b) had absorption peaks at 1650 cm^{-1}, 1458 cm^{-1} and 1032 cm^{-1}, which represent C=O stretching of amides bond, C-N stretching of amides bond and NH_2 rocking of amides bond, respectively. For curve c, the characteristic peak at 574 cm^{-1} for Fe-O stretching was obviously present, then implied that MIL-53(Fe)@CdS-PEI was successfully prepared. Fig. 1C displays the UV–vis spectrum of AuNPs and PtNPs. The AuNPs solution exhibited a sharp absorption peak located at 515 nm, and PtNPs solution had no obvious absorption peak due to 3-thiophenemalonic acid serves as a very effective protective agent for the formation of PtNPs (Sun et al., 2006). For efficient ERET, spectral overlap between the emission spectra of the CdS QDs and absorption spectra of the AuNPs is essential. As Fig. 1D shown, the CdS QDs showed a FL emission peak at 517 nm, whereas the AuNPs exhibited a dominant plasmon absorption peak at about 515 nm, so CdS QDs and AuNPs had a considerable spectral overlap.

3.2. Investigation of the nanogears

The proposed gears A and B was confirmed the formation of the individual gears by native polyacrylamide gel electrophoresis (native PAGE, Fig. 2). As depicted in Fig. 3, lane 2 (circle C + A1) and lane 4 (circle C + B1-AuNPs) posed higher position than lane 3 (circle C), due to circle C had lower molecular weight. Similarly, we could prove that lane 1 (gear A) and lane 5 (gear B) with lower mobility because it had stable structures comparing with lane 2 and lane 4. When gear A and gear B was linked one or two end which would present different electrophoretic mobilities, because the gears were adopted different conformations and different molecular weight. Three single-linked gears (lane 6, lane 8 and lane 10) and two double-linked gears (lane 7 and lane 9) also had a similar mobility, respectively, but the two double-linked gears had slower mobility than single-linked gears due to the higher molecular weight.

3.3. Electrochemical and ECL responses of the modified electrode

To evaluate the electrochemical behavior of aptasensor, CVs and EIS for the modified electrodes were investigated. Combined with Fig. S2A

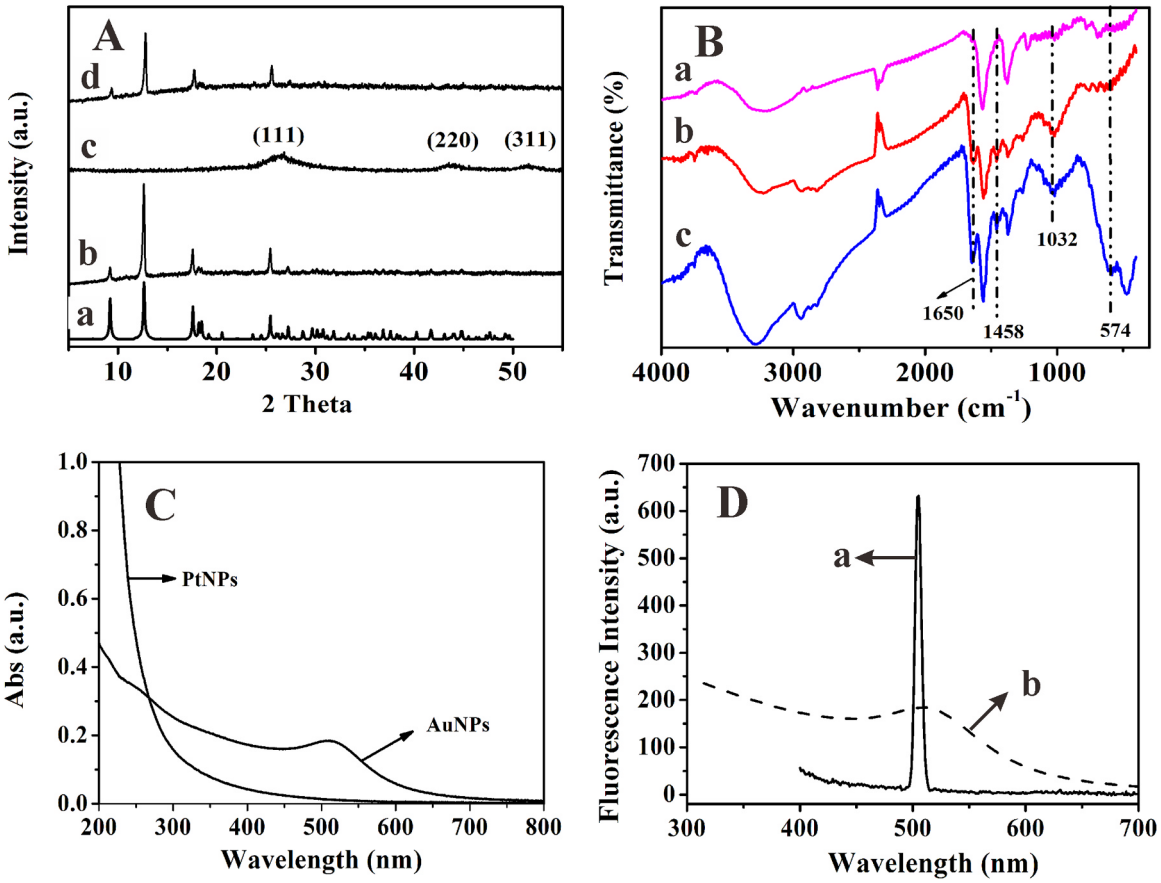

Fig. 1. (A) XRD patterns of a. simulated MIL-53(Fe), b. synthesized MIL-53(Fe), c.CdS QDs and d.MIL-53(Fe)@CdS-PEI, (B) FTIR spectra of a. CdS QDs, b. CdS QDs-PEI and c. MIL-53(Fe)@CdS-PEI, (C) UV-vis spectrum of AuNPs and PtNPs, (D) fluoresence emission spectrum of CdS QDs (a) and absorption spectrum of AuNPs (b).

and S2B, the current of MIL-53(Fe) (curve b) was higher and the impedance was lower than GCE (curve a), because MIL-53(Fe) has good ability of electron transfer. The current of MIL-53(Fe)@CdS-PEI (curve c) was the highest and the impedance was the lowest, due to the good conductivity of CdS QDs. As curve d shown, gear A was modified on MIL-53(Fe)@CdS-PEI, gear A were DNA with poor electrical conductivity, so the current became smaller and the impedance became higher. BSA was macromolecular substance and it's poor conductivity, which leads to the current and impedance were worst (curve e). As curve f shown, the current of MIL-53(Fe)@CdS-PEI/gear A/BSA/aptamer 1-PtNPs was increased compared to MIL-53(Fe)@CdS-PEI/gear A/BSA, and the impedance was reduced, because the PtNPs which modified on the aptamer enhanced electron transport.

Fig. 3 summarized the ECL performance of the aptasensor. When GCE was modified with MIL-53(Fe)@CdS-PEI/gear A (curve a), a significant ECL signal was appearing. When BSA and aptamer 1-PtNPs (curve b) were modified on above electrode, the ECL intensity decreased remarkably, because the BSA was macromolecular material with poor electrical conductivity. The introduction of gear B (curve c), the ECL signal was further descended due to the shortened distance

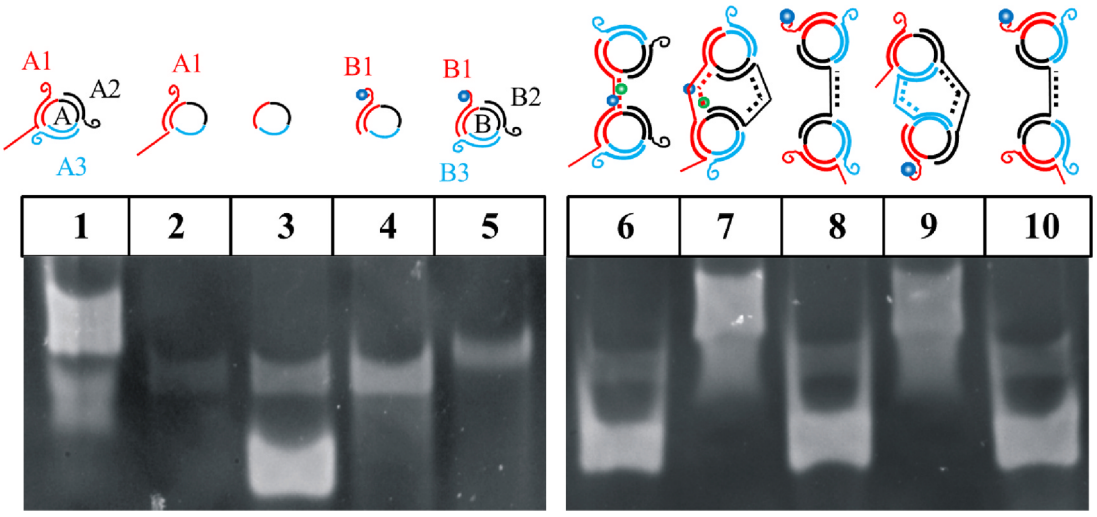

Fig. 2. Formation of individual gears analyzed by 20% native PAGE, the content of each lane is indicated above the lane.

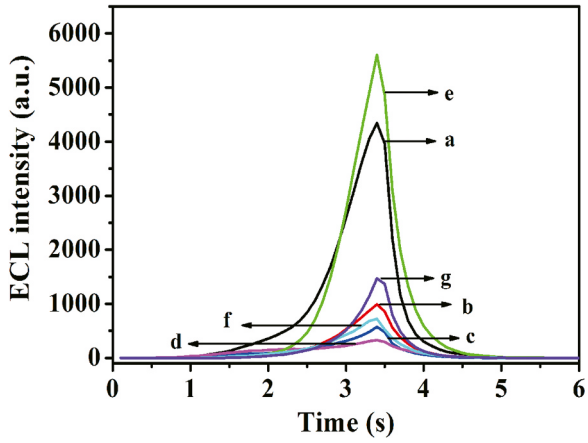

Fig. 3. ECL-time curve of a. MIL-53(Fe)@CdS-PEI/gear A, b. MIL-53(Fe)@CdS-PEI/gear A/BSA/aptamer 1-PtNPs, c. MIL-53(Fe)@CdS-PEI/gear A/BSA/aptamer 1-PtNPs/gear B, d. MIL-53(Fe)@CdS-PEI/gear A/BSA/aptamer 1-PtNPs/gear B/L1, e. MIL-53(Fe)@CdS-PEI/gear A/BSA/aptamer 1-PtNPs/gear B/L1/kanamycin, f. MIL-53(Fe)@CdS-PEI/gear A/BSA/aptamer 1-PtNPs/gear B/L1/kanamycin/aptamer 2, g. MIL-53(Fe)@CdS-PEI/gear A/BSA/aptamer 1-PtNPs/gear B/L1/kanamycin/aptamer 2/neomycin.

between AuNPs and CdS QDs making AuNPs quenching the ECL intensity. When L1 was modified, the ECL signal was lowest due to the double quench property of B1-AuNPs and aptamer 1-PtNPs towards CdS QDs (curve d), then the aptasensor switched to the "off". Subsequently, when the aptasensor switched to "on" state by the addition of kanamycin (curve e), the ECL enhancement was produced due to the SPR of AuNPs between CdS QDs. As curve f shown, when aptamer 2 was introduced to MIL-53(Fe)@CdS-PEI/gear A/BSA/aptamer 1-PtNPs/gear B/L1/kanamycin, the proposed aptasensor switched to "off" again, the distance between AuNPs and CdS QDs became shorter again, resulting in AuNPs quenching the ECL intensity. Finally, the aptasensor switched to "on" state again by the addition of neomycin (curve g), the ECL signal was enhanced by the SPR of AuNPs between CdS QDs.

3.4. Optimization of experimental parameters

Some key factors that influence the ECL response was studied, including the amount of CdS QDs, amount of MIL-53(Fe)@CdS-PEI, amount of aptamer 1- PtNPs, amount of gear B, scan rate and amount of aptamer 2.

When synthesized the MIL-53(Fe)@CdS-PEI composite, the adding amount of CdS QDs was investigated. As shown in Fig. S3A, the ECL intensity increased as the amount of CdS QDs increased from 2.4 to 4.0 mg, but decreased at larger amount. This suggested that the binging between CdS QDs and PEI were limited, excessive CdS QDs cause accumulation, or the ECL emission may be absorbed or scattered (Feng et al., 2018). Consequently, 4.0 mg was chosen as the optimal amount of MIL-53(Fe)@CdS-PEI.

As Fig. S3B shown, the ECL intensity increased with the increasing amount of MIL-53(Fe)@CdS-PEI, up to 3.0 μL, but decreased with larger amounts. This is probably because higher amounts of MIL-53(Fe)@CdS-PEI leading to the thick film which impeded the transfer of electrons. Therefore, 3.0 μL of MIL-53(Fe)@CdS-PEI was chosen for sensor preparation.

The relationship between the amount of aptamer 1- PtNPs and ECL intensity was shown in Fig. S3C, the ECL intensity gradually decreases as the amount of aptamer 1- PtNPs increased from 16 to 24 μL, and the quenching value of ECL intensity enhanced gradually. This suggested that the distance between PtNPs and CdS QDs was less than 10 ± 2 nm, so made the ECL of CdS quench by PtNPs. When excessive aptamer 1-PtNPs was modified on electrode, the distance between some of the PtNPs and the CdS QDs becomes longer thereby weakened the ERET effect resulted in lower ECL quenching response. Thus, the lowest ECL intensity was obtained by 20 μL aptamer 1- PtNPs, which was chosen for experiment due to the strongest ERET effect bewteen QDs and PtNPs.

The amount of gear B modified on the electrode had a quenching effect to the ECL intensity (Fig. S3D). The ECL intensity was gradually decreases with amount of gear B varied from 12 to 16 μL, it was probably because of the short distance between dual metal nanoparticles (AuNPs and PtNPs) and CdS QDs, then the AuNPs and PtNPs were quenching the ECL intensity obviously. With the constant addition of the gear B larger than 16 μL, some aptamer 1-PtNPs was stacked on the electrode surface, then SPR effect was occurring bewteen AuNPs and the CdS QDs due to the distance became longer. Hence, 16 μL of aptamer 1-PtNPs was chosen as the optimal amount of gear B.

As shown in Fig. S3E, the scan rate can affect the ECL intensity over a wide range. The ECL intensity increased with the scan rate was increased from 80 to 100 mV s^{-1}, probably because the ECL of CdS QDs can be trigged at low potential. With the scan rate increased over 100 mV s^{-1}, the ECL intensity was decreased, suggesting that the faster scan rate was unfavorable for hole injection of CdS QDs (Liang et al., 2011). Accordingly, 100 mV s^{-1} was chosen for further experiments.

This experiment also explored the quenching effect of aptamer 2 amount on ECL intensity (Fig. S3F). The quenching value of ECL intensity increased with increasing amount of aptamer 2, and the ΔECL reached maximum at 12 μL, but ΔECL decreased with larger amounts. Due to the introduction of aptamer 2, gear A and gear B were closed again on the surface of the modified electrode, so that the AuNPs of the gear B quenching ECL intensity. But the larger amounts of aptamer 2 impeded the transfer of electrons and the transformation of ground state/excited state of CdS QDs. Thus, 12 μL of aptamer 2 was chosen for aptasensor preparation.

3.5. Mechanism for the ECL system

This ECL aptasensor involved the modification of GCE by MIL-53(Fe)@CdS-PEI, DNA gears and aptamers were assembled in layers to construct a dual gear for kanamycin and neomycin detection. The as-prepared MIL-53(Fe)@CdS-PEI composite generated strong and stable ECL response in the presence of co-reactant $K_2S_2O_8$. This was an "oxidative-reductive" system involving CdS QDs and $K_2S_2O_8$, ECL was produced upon concomitant reduction of CdS QDs and $S_2O_8^{2-}$. The coreactant $S_2O_8^{2-}$ was reduced to the strong oxidant $SO_4^{\bullet-}$, which then reacts with the reduced CdS QDs to generate light. The corresponding ECL processes were listed as followed (Jie et al., 2007):

$$\text{CdS QDs} + ne^- \rightarrow n\,\text{CdS}^{\bullet-} \quad (1)$$

$$S_2O_8^{2-} + e^- \rightarrow SO_4^{2-} + SO_4^{\bullet-} \quad (2)$$

$$\text{CdS}^{\bullet-} + SO_4^{\bullet-} \rightarrow \text{CdS}^* + SO_4^{2-} \quad (3)$$

$$\text{CdS}^* \rightarrow h\nu + \text{CdS} \quad (4)$$

In the absence of target, the close distance between CdS and AuNPs (or PtNPs), CdS^* do not emit photons because all the excitation energy was dissipated in AuNPs (or PtNPs) in ERET processes (Eq. (3)) (Shan et al., 2009). In the presence of target, SPR effect of nanostructure metallic particles caused strongly enhanced local fields, which could lead to a considerable increase of the excitation rate of CdS^* (Eq. (4)) (Liu et al., 2011).

3.6. Analytical performance of the ECL aptasensor

This aptasensor was applied to determine kanamycin and neomycin under the optimal experimental condition. The relative ECL intensity (ΔI) exhibited a linear response to the logarithmic kanamycin concentration in the range 10^{-9}-10^{-5} M (Fig. 4A lina a); the correlation coefficient was 0.9958, the calibration curve $\Delta I = 1262\ \lg c_{\text{kanamycin}}$

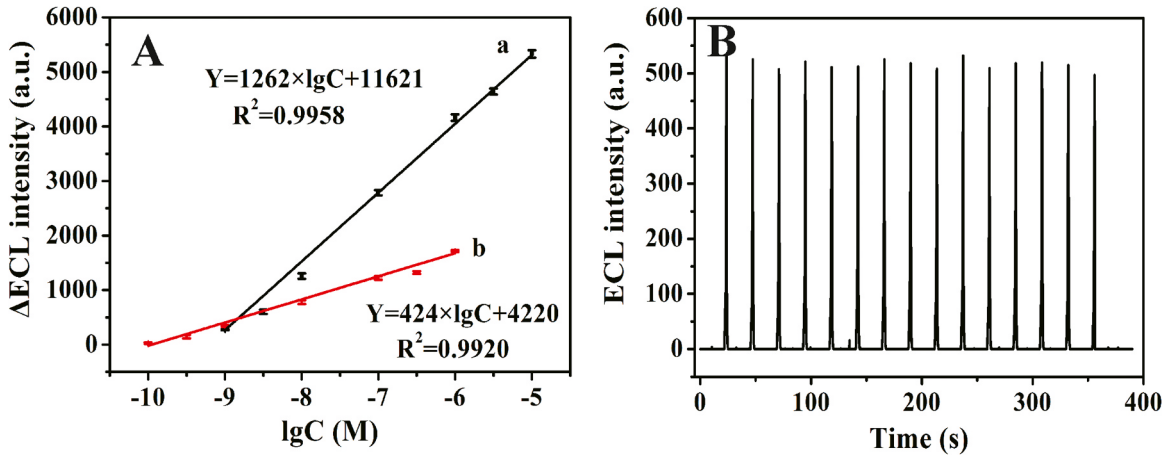

Fig. 4. (A) Calibration curve of ECL intensity versus logarithmic kanamycin (a) and neomycin (b) concentration and (B) ECL emission for 15 continuous cycles.

+ 11,621; the detection limit was 3.5×10^{-10} M. And theΔI exhibited a linear response to the logarithmic neomycin concentration in the range 10^{-10}–10^{-6} M (Fig. 4A line b); the correlation coefficient was 0.9920, the calibration curve $\Delta I = 424\ lgc_{neomycin} + 4220$; the detection limit was 1.7×10^{-11} M. All detection limit determined by the standard Method II of Loock and Wentzell (2012). And, as shown in Fig. 4B, the relative standard deviation (RSD) for ECL emission for 15 continuous cycles was 2.62%, which indicating good reproducibility.

We also investigated the stability and reproducibility of aptasensor, since these were important characteristics of a sensor. The RSD for seven different electrodes constructed by the same procedure was 2.77% (Fig. S4A). Furthermore, aptasensor stability was assessed by determining 10^{-9} M kanamycin and neomycin solutions after 15 days. The ECL intensity remained at 91% and 88% of their original response, respectively. Thus showing good stability and reproducibility for this aptasensor for detecting kanamycin and neomycin. Then, the aptasensor were used for three cycle detections to the analyze the two antibiotics, the RSD for ECL intensity of three cycles was 3.49% (Fig. S4B). This result indicated that the aptasensor possessed desirable regenerability.

Next we investigated selectivity experiments with other antibiotics, including penicillin and chloramphenicol. As shown in Fig. S5A, penicillin and chloramphenicol had little effect at a concentration of 1.0×10^{-7} M, and just resulted in an ECL intensity change of 5%. This result indicated that the aptasensor possessed high selectivity for detection of kanamycin and neomycin. At the same time, this experiment also investigated the interference of various ions to the aptasensor. As Fig. S5B shown, tolerable concentration ratios for interference at the 5% level were 1000 fold for Na^+ (a), K^+ (b), Cl^- (c), NH_4^+ (d), 500 fold for Ca^{2+} (e), Mg^{2+} (f), CO_3^{2-} (g), SO_4^{2-} (h) and 100 fold for ascorbic acid (i).

3.7. Comparison with other methods for the determination of kanamycin and neomycin

The analytical performance of this aptasensor for detection of kanamycin and neomycin were compared with other methods (Table 1). The developed aptasensor was better that other methods due to the present of wider linear range and lower detection limit.

3.8. Application of the ECL aptasensor for determining kanamycin and neomycin in food samples

The proposed aptasensor were used to detection for kanamycin and neomycin in milk and honey were investigated. As shown in Table S2, none kanamycin and neomycin were detected in milk and honey samples, the recoveries of kanamycin were in the range of 95–101% for milk samples, and 99–103% for honey; the recoveries of neomycin were in the range of 100–106% for milk samples, and 99–105% for honey. The recoveries were good that indicated these samples demonstrate the broader potential applicability of this aptasensor for the determination of kanamycin and neocycin in food samples.

To evaluate the applicability of the proposed aptasensor, we compared the results with those obtained by LC-MS. As illustrated in Table S4, the assay results using two methods agreed well with each other.

Table 1
Comparison of the other methods for the detection of kanamycin and neomycin.

Target	Method	Linear range (M)	Detection limit (M)	Reference
Kanamycin	Spectrophotometric	1.0×10^{-9}–5.0×10^{-7}	1.0×10^{-9}	(Zhou et al., 2014)
	Chemiluminescence	2.0×10^{-7}–1.5×10^{-4}	1.4×10^{-7}	(Leung et al., 2013)
	Photoelectrochemical	8.6×10^{-7}–2.4×10^{-4}	3.4×10^{-7}	(Lv et al., 2017)
	HPLC-MS	8.6×10^{-7}–8.6×10^{-5}	1.2×10^{-7}	(Perez and Chen, 2018)
	Colorimetric	3.4×10^{-9}–1.3×10^{-8}	3.4×10^{-9}	(Ha et al., 2017)
	Electrochemiluminecence	1.0×10^{-9}–1.0×10^{-5}	3.5×10^{-10}	This work
Neomycin	Electrochemical	9.0×10^{-9}–7.0×10^{-6}	7.6×10^{-9}	(Lian et al., 2013)
	Fluorescence	1.0×10^{-7}–1.0×10^{-5}	1.0×10^{-8}	(Ling et al., 2016)
	Colorimetric and fluorometric	1.0×10^{-7}–1.0×10^{-6}	2.6×10^{-7}	(Zhou et al., 2013)
	HPLC-MS	1.8×10^{-6}–2.8×10^{-4}	8.8×10^{-7}	(Zu et al., 2018)
	Electrochemiluminecence	1.0×10^{-10}–1.0×10^{-6}	1.7×10^{-11}	This work

4. Conclusions

We have constructed a sensitive and renewable ECL aptasensor based on MIL-53(Fe)@CdS QDs-PEI for determination of multiple antibiotics by DNA gears. This sensor presented a wide range of concentrations, low detection limit, good reproducibility, and good recoveries from milk and honey. This study proved the aptasensor with distance-based ECL response, and provides a promising sensing platform for multiple antibiotics analysis in real samples.

Acknowledgements

The project was supported by the National Natural Science Foundation of China (Nos. 21365004), The Key Research and Development Project of Guangxi (AB18126048), Specific Research Project of Guangxi for Research Bases and Talents (AD18126005), Guangxi Natural Science Foundation (Nos. 2013GXNSFDA019006, 2016GXNSFBA380201, 2018GXNSFAA138086), Young and middle-aged teachers basic ability promotion project by Guangxi Education Department (KY2016YB134), State Key Laboratory of Analytical Chemistry for Life Science, Nanjing University (SKLACL1810).

Declaration of interests

The authors declare that they have no known competing financial interests or personal relationships that could have appeared to influence the work reported in this paper.

Credit author statement

Defen Feng and Yeyu Wu conceived and designed the experiments. Defen Feng performed most of the experiments, contributed to experimental design, data analysis and wrote the manuscript. Chenhao Ai and Yanni Luo performed biological experiment and served the validation. Quanyou Chen supplied resources of samples in this study. Xuecai Tan and Heyou Han designed and supervised the study. All authors discussed the results and commented on the manuscript.

Appendix A. Supporting information

Supplementary data associated with this article can be found in the online version at doi:10.1016/j.bios.2018.12.050.

References

Deng, L., Du, Y., Xu, J.J., Chen, H.Y., 2014. Biosens. Bioelectron. 59, 58–63.
Eddaoudi, M., Kim, J., Rosi, N., Vodak, D., Wachter, J., O'Keeffe, M., Yaghi, O.O., 2002. Science 295, 469–472.
Fan, G.C., Zhu, H., Shen, Q., Han, L., Zhao, M., Zhang, J.R., Zhu, J.J., 2015. Chem. Commun. 51, 7023–7026.
Feng, D.F., Wu, Y.Y., Tan, X.C., Chen, Q.Y., Yan, J., Liu, M., Ai, C.H., Luo, Y.N., Du, F.K., Liu, S.G., Han, H.Y., 2018. Sen. Actuators B 265, 378–386.
Ha, N.R., Jung, I.P., Kim, S.H., Kim, A.R., Yoon, M.Y., 2017. Process Biochem. 62, 161–168.
Han, F., Jiang, H., Fang, D., Jiang, D., 2014. Anal. Chem. 86, 6896–6902.
Jie, G.F., Liu, B., Pan, H.C., Zhu, J.J., Chen, H.Y., 2007. Anal. Chem. 79, 5574–5581.
Jin, Y., Gao, X., 2009. Nat. Nanotechnol. 4, 571–576.
Leung, K.H., He, H.Z., Chan, D.S.H., Fu, W.C., Leung, C.H., Ma, D.L., 2013. Sens. Actuators B 177, 487–492.
Li, H., Eddaoudl, M., O'Keeffe, M., Yaghi, O.M., 1999. Nature 402, 276–279.
Li, L., Chen, Y., Zhu, J.J., 2017. Anal. Chem. 89, 358–371.
Lian, W., Liu, S., Yu, J., Li, J., Cui, M., Xu, W., Huang, J., 2013. Biosens. Bioelectron. 44, 70–76.
Liang, G., Shen, L., Zou, G., Zhang, X., 2011. Chemistry 17, 10213–10215.
Liang, W., Fan, C., Zhuo, Y., Zheng, Y., Xiong, C., Chai, Y., Yuan, R., 2016. Anal. Chem. 88, 4940–4948.
Ling, K., Jiang, H., Zhang, L., Li, Y., Yang, L., Qiu, C., Li, F.R., 2016. Anal. Bioanal. Chem. 408, 3593–3600.
Liu, L., Xu, X., Lei, J., Liu, Y., Yang, Z., 2011. Thin Solid Films 519, 5582–5587.
Loock, H.P., Wentzell, P.D., 2012. Sens. Actuators B 173, 157–163.
Lv, J., Lei, Q., Xiao, Q., Li, X., Huang, Y., Li, H., 2017. Anal. Methods 9, 4754–4759.
Miao, W.J., 2008. Chem. Rev. 108, 2506–2553.
Neumann, T., Johansson, M.L., Kambhampati, D., Knoll, W., 2002. Adv. Funct. Mater. 12, 575–586.
Oertel, R., Neumeister, V., Kirch, W., 2004. J. Chromatogr. A 1058, 197–201.
Perez, J.J., Chen, C.Y., 2018. Rapid Commun. Mass Spectrom. 32, 1549–1556.
Richter, M.M., 2004. Chem. Rev. 104, 3003–3036.
Shan, Y., Xu, J.J., Chen, H.Y., 2009. Chem. Commun. 905–907.
Stokes, R.J., Macaskill, A., Lundahl, P.J., Smith, W.E., Faulds, K., Graham, D., 2007. Small 3, 1593–1601.
Sun, X.P., Du, Y., Zhang, L.X., Dong, S.J., Wang, E.K., 2006. Anal. Chem. 78, 6674–6677.
Thongchai, W., Liawruangath, B., Liawruangrath, S., Greenway, G.M., 2010. Talanta 82, 560–566.
Tian, Y., Mao, C.D., 2004. J. Am. Chem. Soc. 126, 11410–11411.
Wang, Z.G., Elbaz, J., Willner, I., 2011. Nano Lett. 11, 304–309.
Wu, H., Fan, S., Zhang, W., Chen, H., Peng, L., Jin, X., Ma, J., Zhang, H., 2014. Anal. Methods 6, 497–502.
Xiong, C., Liang, W., Zheng, Y., Zhuo, Y., Chai, Y., Yuan, R., 2017. Anal. Chem. 89, 3222–3227.
Zhang, F., Nangreave, J., Liu, Y., Yan, H., 2014. J. Am. Chem. Soc. 136, 11198–11211.
Zhao, Z., Fan, H., Zhou, G., Bai, H., Liang, H., Wang, R., Zhang, X., Tan, W., 2014. J. Am. Chem. Soc. 136, 11220–11223.
Zhou, G., Wang, F., Wang, H., Kambam, S., Chen, X., 2013. Macromol. Rapid Commun. 34, 944–948.
Zhou, N., Zhang, J., Tian, Y., 2014. Anal. Methods 6, 1569–1574.
Zu, M., Jiang, J., Zhao, H., Zhang, S., Yan, Y., Qiu, S., Yuan, S., Han, J., Zhang, Y., Guo, W., Yang, S., 2018. J. Chromatogr. B 1093, 52–59.